Article

Electronic Structure Optimization of PdZn-Graphitic Carbon Nitride Nanocomposites as Electrocatalysts for Selective CO_2 to CO Conversion

Girma W. Woyessa, Chuan-Hung Chuang, Mohammad Rameez,* and Chen-Hsiung Hung*

Read Online

ACCESS | Metrics & More | Article Recommendations | SI Supporting Information

ABSTRACT: Herein, a novel $PdZn/g$-C_3N_4 nanocomposite electrocatalyst, PdZnGCN, prepared from a facile hydrothermal reduction procedure for an efficient CO_2 to CO conversion has been examined. This composite catalyst reduces CO_2 at a thermodynamic overpotential of 0.79 V versus RHE with a 93.6% CO Faradaic efficiency and a CO partial current density of 4.4 mA cm^{-2}. Moreover, the turnover frequency for PdZnGCN reaches 20 974 h^{-1} with an average selectivity of 95.4% for CO after 1 h and an energy efficiency approaching 59%, which is superior to most reported noble metals and metal alloys as electrocatalysts. The enhanced catalytic activity of this nanocomposite is due to synergistic interactions between PdZn and g-C_3N_4 as evidenced by optimum work function, zeta potential, CO desorption rate, and downshifted d-band center. Furthermore, suppressed grain growth during the formation of nanocomposites also results in faster reaction kinetics, as demonstrated by a lower Tafel slope (93.6 mV/dec) and a larger electrochemically active surface, consequently enhancing the overall performance.
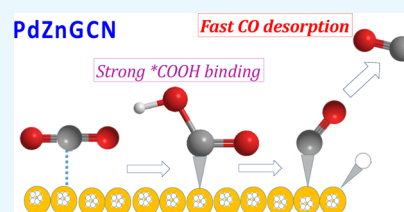
INTRODUCTION

The increase in fossil fuel consumption has led to a growing urgency to reduce carbon dioxide emissions and develop sustainable energy technologies.[1,2] Recently, research to find an alternative energy source by converting CO_2 into carbon-neutral fuels has been intensified. Electrochemical reduction is attractive as it can employ green electrolytes, utilize surplus electricity from renewable energy resources, and adjust device performance through optimization of catalysts.[3,4] However, the electrochemical CO_2 reduction reaction (ECO$_2$RR) still suffers from high overpotential, low selectivity, and poor long-term stability due to the high thermodynamic stability of CO_2 and competing hydrogen evolution reactions.[5] Hence, developing an efficient electrocatalyst to achieve both a high Faradaic efficiency (FE) and a sizeable current density is of urgent importance, although it is still very challenging.[6]

Lately, carbon-based nanomaterials have been extensively reported as the electrocatalysts for CO_2 reduction.[2] Among various carbon materials, two-dimensional graphitic carbon nitride (g-C_3N_4) has shown promising activities in electrocatalytic processes, such as HER,[7] OER,[8] and ECO$_2$RR,[9] with advantages of low cost, high stability, ease of synthesis, and environmental benignity. In addition, g-C_3N_4 could serve as an ideal molecular scaffold to prepare nanocomposites for electrochemical CO_2 reduction since the abundant "nitrogen pockets" on the fringes of heptazines lead to improved CO_2 retention and metal inclusions.[10] Moreover, the carbon atoms in g-C_3N_4 exhibit high oxophilicity, which is beneficial for stabilizing intermediates.[11] So far, the applications of pristine g-C_3N_4 in electrochemical CO_2 reduction have been barely

appreciated due to its inherent low conductivity, impotent active sites, and lack of detailed mechanistic information.[9] These problems have been partially amended by incorporating g-C_3N_4 with other carbonaceous materials such as single or multi-walled carbon nanotubes and carbon quantum dots, although doping with additional precious metals such as Au or Ag to boost its catalytic performance is usually required.[11−13] Metals and metal oxides have also been incorporated with g-C_3N_4 to form composite materials. Using Cu-decorated g-C_3N_4 for electrochemical CO_2 reduction, Qiao et al. observed hydrogen (>50%) as the major gaseous product with a significantly higher selectivity for C2 products than from conventional Cu supported on nitrogen-doped graphene.[11]

Recently, our group has reported bimetallic copper−iron mixed oxides for electrochemical CO_2 reduction to CO with a maximum FE of 84.4% at −1.6 V versus Ag/AgCl. Nonetheless, composite materials composed of metal oxides and g-C_3N_4 still exhibit relatively high overpotentials.[14] Another viable strategy is to employ metal alloy-based g-C_3N_4 composites for ECO$_2$RR, taking advantage of enhanced conductivity and a strong synergistic effect between the metals of the alloy.[15,16] The composition of alloys and g-C_3N_4 can further boost the catalytic activities through strain engineering,
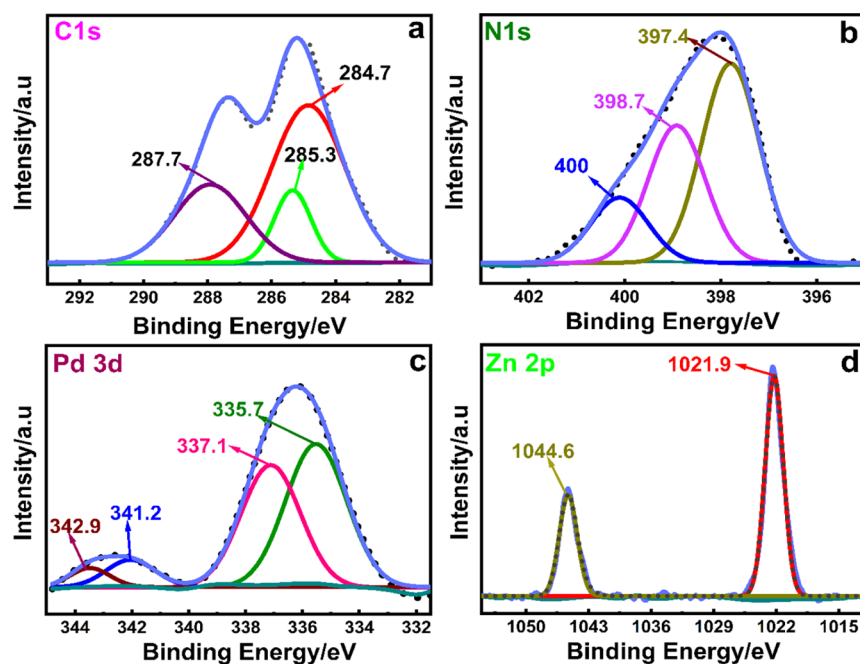
Figure 1. XPS spectra: core transitions and fitting of (a) C 1s, (b) N 1s, (c) Pd 3d$_{3/2}$, and (d) Zn 2p$_{3/2}$ for PdZnGCN. (Note: solid black dots represent the experimental data, solid color lines show peaks from deconvolution, and light blue lines are the sum of fitted transitions).
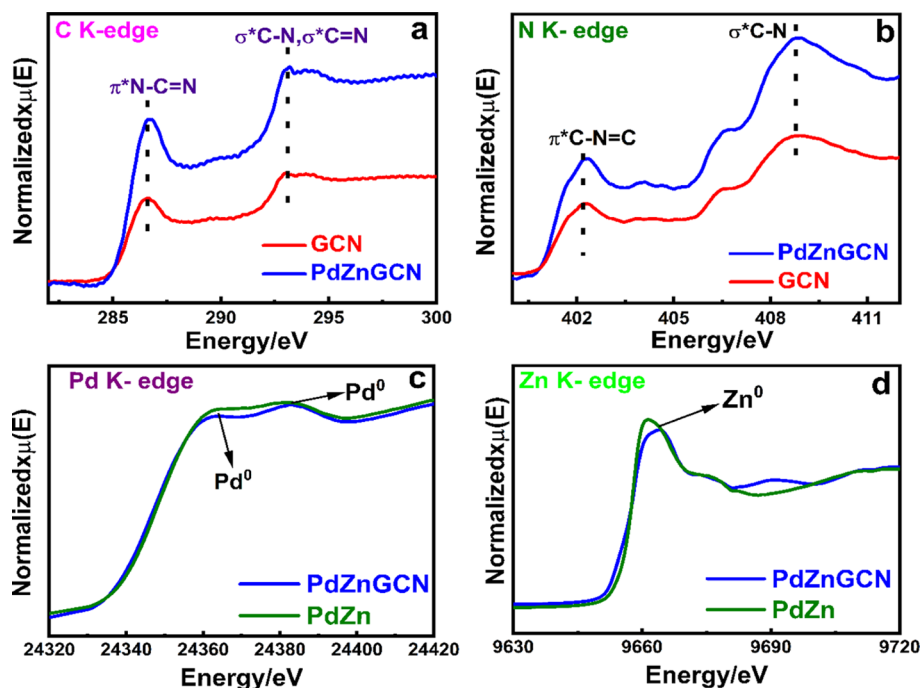

Figure 2. XANES spectra of the (a) C K-edge and (b) N K-edge for GCN and PdZnGCN and EXAFS spectra for the (c) Pd K-edge and (d) Zn K-edge for PdZnGCN and PdZn.

tuning of d-band centers, and modulation of work functions.[2,17−19] The PdZn alloy has been applied as a catalyst for ECO$_2$RR but only exhibits moderate performance with low stability and low current densities.[19,20] To bridge the gap, we prepared the PdZn/g-C$_3$N$_4$ nanocomposite (hereafter denoted as PdZnGCN) by a simple hydrothermal reduction reaction and compared the ECO$_2$RR activities among PdZnGCN, pure g-C$_3$N$_4$ (denoted as GCN), and PdZn. The composite PdZnGCN with a metal loading of 4 wt % showed the highest catalytic activity to convert CO$_2$ to CO with an average FE of 93.6% and an impressive CO partial current density of 4.4 mA cm^{-2} at a thermodynamic overpotential of 0.79 V. Additionally, PdZnGCN showed good stability with steady performance for three consecutive reaction cycles. We attributed the superb catalytic activity of PdZnGCN to its large electrochemically active surface area, d-band center shift, optimum work function, and strain engineering achieved through synergistic interactions between PdZn and g-C$_3$N$_4$.

■ RESULTS AND DISCUSSION

Characterizations of the PdZnGCN Nanocomposite.
Bulk graphitic carbon nitride, prepared by direct heating of the dicyandiamide precursor, was chemically exfoliated to obtain pure g-C_3N_4. The catalysts PdZnGCN and PdZn were synthesized by hydrothermal processes. The detailed steps for preparing these materials are provided in the Supporting Information. The composition and valence states of PdZnGCN were confirmed by high-resolution X-ray photoelectron spectra (HR-XPS) presented as different energy regions in Figure 1a−d and as a full survey spectrum in Figure S1. As shown in Figure 1a, the C 1s spectrum at 284.7 eV can be ascribed to sp2 carbons in the graphitic carbon nitride, while the peaks at 285.3 and 287.7 eV are assigned to carbons on C−N−C and N−C≡N units of g-C_3N_4.[14] The N 1s peak of PdZnGCN could be deconvoluted to three peaks (Figure 1b), with 398.7 eV corresponding to the sp^2 hybridized N of the N≡C bonds, 400.1 eV attributed to amino functional groups (N−H), and 397.4 eV assigned to N in C≡N−C.[14] As displayed in Figure 1c for the XPS Pd 3d region of PdZnGCN, the binding energies at 335.7 and 341.2 eV are Pd(0) photoelectrons from the $3d_{5/2}$ and $3d_{3/2}$ core-level, respectively.[21] Additional two Pd(II) peaks, 337.1 and 342.9 eV, should originate from the PdZnGCN composite's surface oxidation.[22] As shown in Figure 1d, the Zn 2p peaks, composed of 1021.9 and 1044.6 eV, can be assigned to Zn $2p_{3/2}$ and Zn $2p_{1/2}$ of Zn(0), respectively.[23] Notably, the binding energies of C 1s, N 1s, Pd 3d, and Zn 2p for the PdZnGCN nanocomposite are slightly lowered by 0.27, 0.22, 0.15, and 1.45 eV, respectively, compared to the corresponding g-C_3N_4 or PdZn alloy particles (Figure S2a−d), and the differences can be attributed to strong electronic interactions between g-C_3N_4 and PdZn. These electronic interactions, as further evidenced by data from XRD, IR, and XPS (vide infra), might be crucial to control the product selectivity of ECO_2RR through tuning the binding strength of intermediates and, accordingly, enhancing the rate of CO release.[24]

The shifts of absorption edges in X-ray absorption near-edge structures (XANES) spectra provide additional information on electronic interactions between g-C_3N_4 and bimetallic nanoparticles in PdZnGCN. The characteristic C K-edge peaks at 286.6 and 293.0 eV, shown in Figure 2a, were assigned to electronic transition from the C 1s to 2p π^* orbitals in the pyridine-like C≡N bonds[25] and to σ^* in C−N and C≡N bonds.[26]

In the N K-edge spectra, the peak at 402.1 eV for GCN was attributed to the π^* graphitic N moieties, while the corresponding peak for PdZnGCN appeared at 402.3 eV (Figure 2b). The increases in peak intensities from GCN to PdZnGCN in carbon and nitrogen K-edge spectra suggest electronic interactions between PdZn and g-C_3N_4.[27] Besides, the shifting of photon energies of PdZnGCN to higher values in both C and N spectra indicates electron transfer occurred from g-C_3N_4 to PdZn.[28] Figure 2c,d shows two characteristic peaks from metallic Pd at around 24 360 and 24 383 eV,[29] while metallic zinc showed a peak at 9662 eV.[30] Slight decreases in peak intensities were observed in the spectrum of PdZnGCN due to interactions between PdZn and g-C_3N_4. These interactions are critical for enhancing charge migration in the PdZnGCN composite and improving the catalytic activity and stability.[31]

The identities of GCN, PdZnGCN, and PdZn were further verified through comparisons of powder X-ray diffractions (PXRD) shown in Figure S3a. After incorporating PdZn, the diffraction peaks at 12.8 and 27.8° from g-C_3N_4 were still well-observed, which confirms that the original molecular structure of g-C_3N_4 was retained.[32] The PXRD pattern of PdZnGCN exhibited characteristic diffraction peaks of (111), (200), and (220) at 40.3, 46.9, and 68.6°, respectively, suggesting the presence of PdZn nanoparticles (COF #1522606). The intense diffraction peaks from PdZn reflect the high crystallinity of the alloy compared to g-C_3N_4. Additionally, slight shifts in the 2θ values and minor peak broadening are noticed in the PXRD diffractogram of PdZnGCN (Figure S3b). These shifts might be correlated with a compressive strain that will enhance the activity of ECO_2RR of PdZnGCN through tuning the electronic structure.[17,18] The origin of this compressive strain could be attributed to different nucleation and crystallization rates of PdZn, which alter the size of PdZn particles in the presence of g-C_3N_4. Consequently, due to smaller particle sizes, this compressive strain governed by the Young−Laplace equation will be able to downshift the d-band center, alter the adsorption energy, and, consequently, control the overall ECO_2RR.[17,18,33]

The SEM image of the as-prepared PdZnGCN, as shown in Figure S4a, indicated fine particles of PdZn distributed on the surface of graphitic carbon nitride. The TEM images of PdZnGCN revealed that bimetallic PdZn nanoparticles were roughly spherical with a mean diameter of 5.47 ± 2.03 nm dispersed on g-C_3N_4 nanosheets (Figure S4b,c). Aggregation of the nanoparticles occurred during the heating process under hydrothermal conditions.[34] The high-resolution transmission electron microscope (HRTEM) image of PdZnGCN in Figure S4d shows metal clusters with lattice spacings of 0.223 and 0.195 nm, which are in good agreement with a face-centered cubic PdZn lattice for PdZn(111) and (200) planes, respectively, calculated from the CIF file of the Crystallography Open Database (COF #1522606) with a reported formula of $Pd_{0.81}Zn_{0.19}$. Noticeably, the lattice fringes from the HRTEM of PdZnGCN are well consistent with the lattice spacing calculated from the PXRD diffractogram.

The SEM and HRTEM elemental mappings of PdZnGCN carried out by energy-dispersive X-ray spectroscopy (EDX), as shown in Figures S5 and S6, demonstrated that the nanocomposite exhibits well-dispersed Pd and Zn elements from PdZn nanoparticles on the surface of uniformly distributed C and N elements of g-C_3N_4. The g-C_3N_4 nanosheets provide the frameworks on which these alloy particles are anchored. In addition, each element is evenly scattered without elemental segregation or the formation of immiscible phases. The mole ratio of Pd to Zn obtained from TEM−EDX (3.86:1), as presented in Figure S7, is in close agreement with the value of 4.3:1 calculated from the reported formula of $Pd_{0.81}Zn_{0.19}$ in the PXRD database. Furthermore, based on the data of inductively coupled plasma−optical emission spectrometry (ICP-OES) shown in Table S1, Pd and Zn sum up to a 4% total weight content in the sample of PdZnGCN.

Performance of PdZnGCN as a Cathodic Electro-catalyst for ECO_2RR. The electrochemical CO_2 reduction activity using PdZnGCN mixed with Nafion sprayed on carbon cloth as the working electrode was investigated by linear sweep voltammetry (LSV) in Ar or CO_2-saturated 0.1 M KCl electrolyte (pH = 6.92) and compared with results obtained
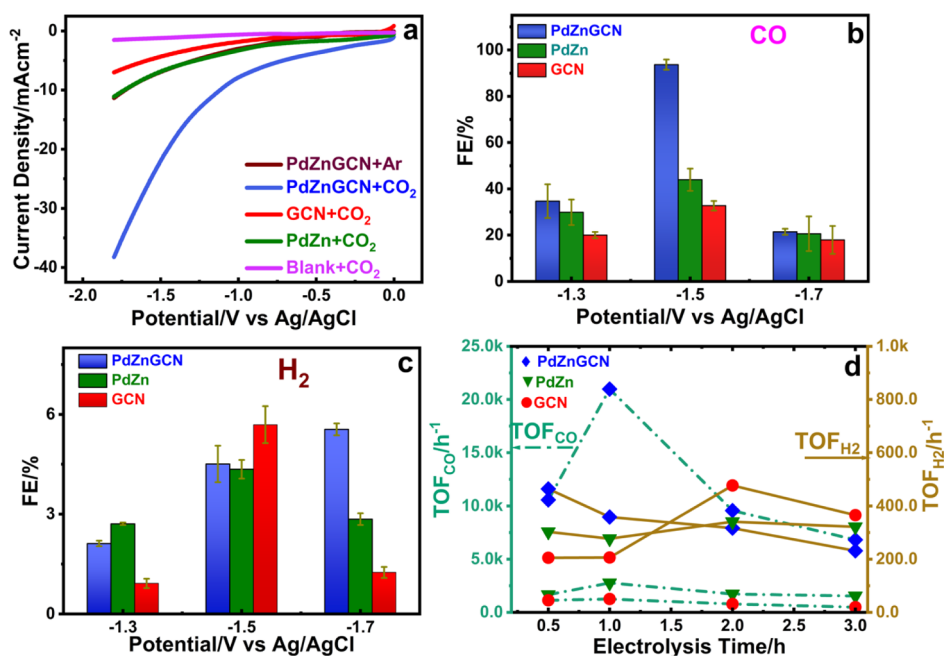
Figure 3. (a) Linear sweep voltammograms with carbon cloth (blank), PdZn, and GCN measured under saturated CO_2 and PdZnGCN measured under both saturated CO_2 and Ar; (b) Average FE for CO at −1.3, −1.5, and −1.7 V after electrolysis for 1 h; (c) Average FE for H_2 at −1.3, −1.5, and −1.7 V after electrolysis for 1 h; (d) Average TOF for CO and H_2 at −1.5 V.

from either PdZn or GCN as the catalyst. As illustrated in Figure 3a, the reductive current rose sharply to over 8 mA/cm^2 as the potential swept to more negative than −0.9 V versus Ag/AgCl, suggesting a low overpotential for CO_2 reduction using PdZnGCN as the catalyst.[27]

The significantly lower onset potential for the PdZnGCN nanocomposite ensures efficient CO production via the formation of more surface-adsorbed intermediates by lowering the energy barriers and thereby improving the ECO_2RR catalytic activity.[35] On the contrary, only using carbon cloth as an electrode without any catalyst, no such current enhancement was observed under saturated CO_2 conditions in a potential range between 0 and −1.8 V. The catalyst PdZnGCN in the CO_2-saturated electrolyte exhibits approximately 3.45 times and 5.47 times higher current density than that of using PdZn or GCN as the catalyst, respectively, at −1.8 V versus Ag/AgCl. This comparison demonstrated that PdZnGCN is a much more active catalyst toward electrocatalytic CO_2 reduction. A controlled electrolysis under CO_2 using carbon cloth as the working electrode but without the presence of a catalyst leads to a negligible current density of 0.016 mA cm^{-2} at −1.5 V versus Ag/AgCl (−0.9 V vs RHE) with no CO production.

The electrocatalytic CO_2 to CO conversion using PdZnGCN, PdZn, and GCN on carbon cloth as working electrodes was quantified by gas chromatography (GC) equipped with a thermal conductivity detector (TCD). The plots of average charge buildup versus time from electrolysis at different applied potentials are displayed in Figure S8. During the first hour of electrolysis at an applied potential of −1.5 V versus Ag/AgCl, PdZnGCN accumulates 24.0 C of average charges, whereas GCN and PdZn reach only 15.3 and 14.6 C, respectively. The average amounts of CO generated in the headspace under −1.5 V versus Ag/AgCl in 1 h were 2719.0, 726.5, and 1367.4 μL using PdZnGCN, GCN, and PdZn as the catalysts, respectively (Figure S9). Meanwhile, the amount of

H_2 generated from the PdZnGCN electrode under the same conditions was 143.8 μL, followed by 101.3 μL from GCN and 82.3 μL from PdZn. Evidently, the volume ratio of CO to H_2 after 1 h of electrolysis at −1.5 V versus Ag/AgCl of 18.9/1 for PdZnGCN outperformed the values of 7.2/1 and 16.6/1 from using GCN and PdZn as the electrocatalysts, respectively.

Based on charge accumulation and the amount of CO generated, an average FE of 93.6% (±2.2%) for CO production was obtained at an applied potential of −1.5 V versus Ag/AgCl using PdZnGCN as the catalyst (Figure 3b,c), which indicates a near-exclusive selectivity for CO_2 to CO conversion by PdZnGCN. Meanwhile, the FE for H_2 under the same condition was 4.5% (±1.5%), and the total FE of products was 98.1%. Contrastingly, the averaged FEs for CO using PdZn or GCN as the electrocatalyst were only 44% (±5%) and 33% (±2%). Meanwhile, for H_2 production, the FEs are 4.3% (±1.3%) and 5.7% (±2.1%) for PdZn and GCN, respectively. Since no other ECO_2RR product can be detected from GC chromatograms and NMR spectroscopy, we postulate that one of the reasons for less than 100% FE for GCN and PdZn could be the poisoning of the catalytic surface and formation of other side products such as carbonates and bicarbonates.[36]

As shown in Figure S10a−c, the CO partial current densities, j_{CO}, with PdZnGCN as the electrocatalyst for ECO_2RR, reached a maximum value of 4.4 mA cm^{-2} at −1.5 V versus Ag/AgCl. The lower j_{CO} values of 0.7 mA cm^{-2} at −1.7 V and 0.4 mA cm^{-2} at −1.3 V versus AgCl indicate the distinctive potential dependency of partial current densities for CO production. The decrease in j_{CO} at a more negative potential might be related to more surface-bound OH$^-$ intermediates accumulating near the electrode surface to lower the effective concentration of CO_2 near the electrode surface and eventually lead to the decline of the CO partial current density.[37] On the contrary, the partial current densities of j_{H_2} under different applied potentials showed a different

Table 1. Comparison of Catalytic Performance Parameters for Different Catalyst Systems for Reduction to CO (vs RHE)

catalyst	electrolyte	mass (mg/cm^2)	$E_{applied}$ (V vs RHE)	η_{thermo} (V)	j_{CO} (mA/cm^2)	FE$_{max}$ (%)	ref
Ag−S-g-C$_3$N$_4$/CNT	KHCO$_3$ (0.1 M)	0.5	−0.75	−0.64	0.3	91.4	13
Cu$_2$O−FeO/g-C$_3$N$_4$	KCl (0.1 M)	0.6	−0.99	−0.88	3.9	84.4	14
Au−Pd	KHCO$_3$ (0.1 M)		−0.50	−0.40	∼0.2	∼80.0	15
PdAg/C	KHCO$_3$ (0.5 M)	0.6	−0.60	−0.50	3.0	95.3	16
PdZn/CB	KHCO$_3$ (0.1 M)	∼5	−0.60	−0.50		∼10.0	19
PdCu	KHCO$_3$ (0.1 M)	2.0	−0.89	−0.78	6.9	86.0	20
PdZnGCN	**KCl (0.1 M)**	**1.4**	**−0.90**	**−0.79**	**4.4**	**93.6**	**this work**

trend, with the lowest value at −1.5 V versus Ag/AgCl in agreement that the majority of electricity was consumed for electrochemical CO$_2$ conversion to CO.

The turnover frequency (TOF), a vital measure of the per-site activity of catalysts for CO$_2$ reduction, was calculated from eqs S3 to S5 as listed in Supporting Information for the three electrocatalysts and presented as a time-dependent plot in Figure 3d. Noticeably, the averaged TOF value from three trials using PdZnGCN as the catalyst reached a value of 20 974 h^{-1}, which is much higher than 2772 h^{-1} using PdZn and 1261 h^{-1} from GCN as the catalyst. Notably, the TOF value for electrochemical CO$_2$ to CO reduction using PdZnGCN as the catalyst surpasses reported values with the Zn nanosheet (1500 h^{-1}),[5] MoS$_2$ (1209 h^{-1}),[38] or Pd (∼600 h^{-1})[39] as the catalyst. It was two times higher than our previously reported g-C$_3$N$_4$/Cu$_2$O−FeO catalyst (∼10 000 h^{-1}).[14] The high FE (93.6%) and TOFs (20 974 h^{-1}) at −1.5 V versus Ag/AgCl over 1 h indicate the superior performance of PdZnGCN for electrochemical CO$_2$ to CO reduction via a dual enhancement from both the synergistic interactions between Pd and Zn and electronic interactions between PdZn and GCN, which appears to increase CO$_2$ adsorption and lower the CO$_2$ activation energy at the active sites.[40]

To elucidate the complementary ligand effect of atoms in the PdZn alloy, the electrocatalytic CO$_2$ reduction reactions were performed using nanoparticles of a single element, Pd or Zn, incorporated on g-C$_3$N$_4$ as the catalyst, and the resulting data has been summarized in Table S3. The catalyst ZnGCN demonstrated a higher FE (56.1%) for CO production than using PdGCN (21.6%) in addition to a higher partial current density, an electrochemically active surface area (ECAS), and an energy efficiency as compared to PdGCN at −1.5 versus Ag/AgCl. The synergistic effect of the simultaneous presence of palladium and zinc as the alloy along with g-C$_3$N$_4$ has been corroborated to be essential for achieving high FEs of CO. It is worth mentioning that likely due to low activity of Zn toward hydrogen evolution reaction,[3] Zn nanoparticles appear to play a substantial role in product selectivity, which can be evidenced by a higher CO$_2$ to CO FE of 56.1% from ZnGCN than 21.6% from PdGCN and a suppressed HER when ZnGCN was used as the catalyst. Consequently, the strategy of combining the PdZn alloy with 2D g-C$_3$N$_4$ to form the PdZnGCN nanocomposite successfully suppresses the HER activity and enhances the overall selectivity of CO. As shown in Table 1, the PdZnGCN electrocatalyst achieves excellent selectivity, high Faradaic efficiencies, and large partial current density, concurrently, for CO$_2$ to CO conversion compared to other electrocatalysts. This PdZnGCN electrocatalyst, with a low percentage of precious metal loading (4%), has successfully suppressed the unwanted HER to demonstrate the efficacy of this approach.

To further elaborate on the synergistic effects of the PdZnGCN catalyst, we calculated the ECAS (Supporting Information for details) and the exchange current densities (j_0) from the Tafel plot. As shown in Table 2, the ECAS value for

Table 2. Summary of Electrochemical Parameters for Samples in 0.1 M KCl under Saturated CO$_2$

catalyst	ECAS (cm^2)	j_0 (μA/cm^2)
PdZnGCN	1.38	0.07
GCN	1.04	0.02
PdZn	1.17	0.06

PdZnGCN (1.38 cm^2), obtained from the ratio of double-layer capacitance (C_{dl}) and specific capacitance (C_{sp}), was higher than that of PdZn (1.17 cm^2) and GCN (1.04 cm^2), attributed to the smaller nanoparticles of PdZn on the g-C$_3$N$_4$ nanosheets in PdZnGCN. This higher electrochemically active surface area for PdZnGCN favors CO$_2$ adsorption and rapid rate-limiting electron transfer from CO$_2$ to CO$_2$$^{\bullet-}$ resulting in enhanced ECO$_2$RR.[14] The exchange current density (j_0) of 0.07 μA cm^{-2} obtained from the Tafel plot for PdZnGCN was more significant than that of 0.06 μA cm^{-2} for PdZn and 0.02 μA cm^{-2} for GCN. The high exchange current density for PdZnGCN leads to a faster electrochemical reaction and consequently enhanced catalytic performance.[41]

To investigate the long-term stability of the catalysts, a 17 h electrolysis has been performed on electrocatalytic systems using working electrodes fabricated with PdZnGCN, PdZn, or GCN at −1.5 V versus Ag/AgCl. As shown in Figure 4a, a linear increase in charge accumulation with time has been observed in all systems for more than 17 h, indicating good stability of the catalysts. Moreover, the SEM images confirmed that no significant change was observed in electrode morphology for PdZnGCN after long-term bulk electrolysis (Figure S11). The extended X-ray absorption fine structure (EXAFS) for Pd and Zn K-edge also showed no significant change in the spectrum before and after bulk electrolysis reaction indicating the good stability of the catalyst (Figure S12). Lastly, the PdZnGCN electrode was subjected to three consecutive electrolysis at −1.5 V versus Ag/AgCl and showed similar performance for all three cycles (Figure S13). All of these stability tests indicate that the prepared catalysts are very stable and show no significant oxidation or change in morphology, and PdZnGCN can be recycled without degradation in performance.

Besides current density and selectivity, the energy conversion efficiency is also a critical parameter by which any electrocatalyst can be benchmarked for renewable energy storage and fuel synthesis. Hence, we also calculated the energy efficiency of CO$_2$ to CO reduction (ε_{CO}) from FE and overpotential following the eq S7 listed in the Supporting
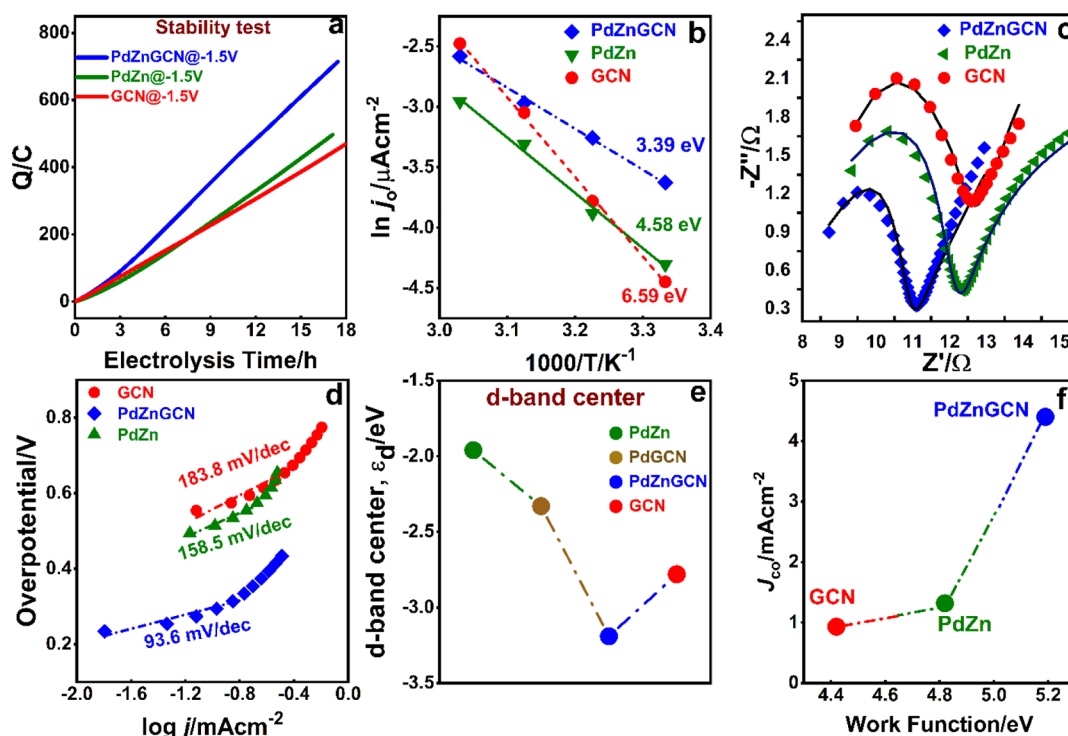
Figure 4. a) Amount of charge accumulated (C) versus electrolysis time (h) for all the catalysts at -1.5 V (vs Ag/AgCl) during 17 h electrolysis; (b) Activation energies of the catalysts; (c) Nyquist plot under 0.1 M KCl and in saturated CO_2; (d) Tafel plots; (e) D-band center measured from UPS in the absence of CO_2; (f) Volcano plot between the work function of all the catalysts versus partial current density for CO after 1 h.

Information. As summarized in Table S2, at an applied potential of -1.5 V versus Ag/AgCl, the energy efficiency of 59% ($\pm1\%$) was obtained for the CO_2 electrocatalytic reduction to CO by PdZnGCN, which is ~2 and ~3 times higher than that of PdZn ($28 \pm 3\%$) and GCN ($20 \pm 1\%$), respectively. The highest energy efficiency observed for PdZnGCN could be due to its higher ECAS and electronic structure optimization.

Rationalizations to Superior Performance of PdZnGCN on ECO$_2$RR. To gain a further mechanistic understanding of the electrocatalytic CO_2 reduction using PdZnGCN as the catalyst and to elucidate the electronic structure tuning in this composite material, the activation energy (E_a) and Tafel slope are calculated. The activation energy (E_a) can be obtained from the plot of logarithmic exchange current density ($\ln(j_0)$) versus reciprocal temperature ($1/T$),[42] as shown in Figure 4b and Table S2. From the slope, the lowest E_a of 3.39 eV for the electrocatalytic reaction using PdZnGCN as the catalyst was obtained compared to the values of 4.58 and 6.59 eV for those of PdZn and GCN, respectively. The smaller activation energy for the reaction that occurred on the PdZnGCN electrode is consistent with enhanced CO_2 adsorption and electronic interaction between PdZn and GCN, which facilitates activation of CO_2 and leads to the highest CO partial current density value and the highest FE.[42]

In order to clarify the rate-determining step and reaction pathway, Tafel analysis was performed by comparing the Tafel slopes of the electrocatalytic reactions obtained from the plots of overpotential versus logarithmic current density.[41] As shown in Figure 4d, the Tafel slopes of PdZnGCN, GCN, and PdZn were 93.6 mV/dec, 183.8 mV/dec, and 158.5 mV/dec, respectively. The smallest Tafel slope of PdZnGCN as the catalyst with the value close to 118 mV/dec suggests that initial

electron transfer to generate a surface-adsorbed $CO_2^{\bullet-}$ species is the more plausible rate-determining step for CO generation as reported earlier for the heterogeneous catalysts.[43]

To investigate the charge transfer kinetics of the catalysts, electrochemical impedance (EIS) spectra are measured, as shown in Figure 4c. The parameters Ohmic resistance (R_s) and charge transfer resistance (R_{ct}) obtained from the EIS fitting with an equivalent circuit model shown in Figure S14 are listed in Table S4.

Notably, the catalyst PdZnGCN displayed a smaller charge transfer resistance (1.99 Ω) than using PdZn (3.20 Ω) or GCN (3.58 Ω) as the catalyst, indicating that the modification of g-C_3N_4 with the PdZn bimetallic nanocomposite could promote electrochemical CO_2 reduction by inducing faster charge transportation and rapid reaction kinetics, hence ensuring the fast electron transfer to CO_2 for the formation of the $CO_2^{\bullet-}$ radical anion intermediate.[38] On the other hand, the larger R_{ct} value for GCN resulted in a longer diffusion path for electron migrations and offered the lowest charge mobility, consequently inhibiting electron transfer from the electrolyte to the electrode GCN.[44] Hence, the PdZnGCN electrode displays an accelerated charge transfer process at the electrode interface and enhances the overall electrochemical CO_2 reduction activity.

The influence of the synergistic effect and strain engineering on the ECO$_2$RR mechanism, d-band center (ε_d), and work function (WF) of all the catalysts has been determined by synchrotron-based UPS measurements and is presented in Figure S15 and Table S5. The synergistic effect and the strain and ligand effect determine the electrocatalytic activity, selectivity, and stability.[33] The d-band center is located at a lower energy level than that of PdZnGCN (-3.19 eV) and shifts away from the Fermi level. Due to the compressive
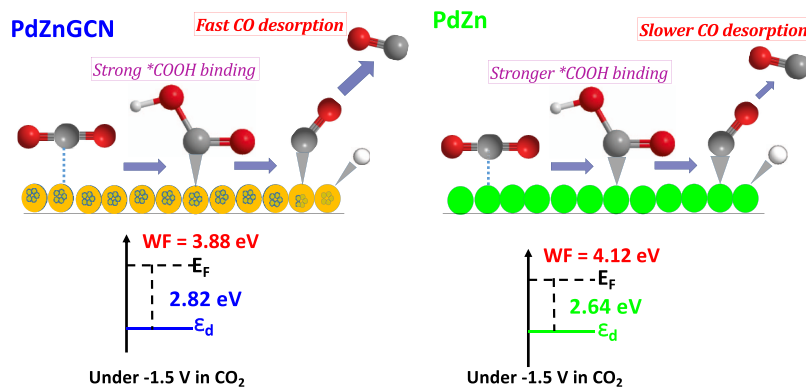
Figure 5. Diagram of the binding energy strength of COOH*, CO*, and H* intermediates on PdZnGCN and as a function of the d-band center under CO_2 and applied potential.

strain, the downward shifting of the d-band center will reduce the interactions with the adsorbates on the catalyst's surface and, therefore, weaken the binding strength of *CO.[18] Owing to the weak binding energies of the adsorbed *CO intermediates, CO can be easily desorbed and consequently enhance the activity and selectivity of the PdZnGCN catalyst.[18] Moreover, the ligand effect exerted by g-C_3N_4 was also visible as the d-band center of PdZnGCN was lower than that of both ZnGCN and PdGCN. This ligand effect, or termed electronic effect, together with the strain effect, enhances the overall energy efficiency and selectivity toward CO. Hence, the PdZn alloy complexing with g-C_3N_4 offers advantageous pathways to tune the electronic properties of an electrocatalyst for selective ECO_2RR.

Work function measurements further confirmed the synergistic effect and electronic tuning. The trend observed in WF of PdZnGCN > PdZn > GCN was consistent with the trends observed in FEs and j_{CO}. The measured work function value of 5.19 eV for using PdZnGCN as the electrocatalyst was higher than that of PdZn (4.82 eV) and GCN (4.42 eV), dictating the synergistic effect via charge transfer interactions. This charge transfer redistributes the interfacial charge, which enhances the selectivity for CO. Gunji et al. recently showed that work function at around 5.32 eV enhances the electrocatalytic selectivity and activity of ECO_2RR using Pd-based composites as the catalyst.[19] The PdZnGCN work function lies closer to this value, accounting for observed selectivity and enhanced activity. On the other hand, the in-operando WF measured under applied potential in the CO_2-saturated catalyst for PdZnGCN (3.82 eV) was lower than that of PdZn (4.12 eV), dictating the lower energetic barrier to donating electrons from the catalyst surface to the adsorbed CO_2, which further facilitates the formation of intermediates to enhance the selectivity of the CO product.

Additionally, we elaborated on the surface behavior of the catalysts. As shown in Figure S16, zeta potential (ζ) measurement confirms that PdZnGCN nanocomposites are more negatively charged than PdZn and GCN alone, which is in good agreement with our XPS and EXAFS results. The Tafel slope is correlated with the surface charge density, that is, the more negative the surface, the more it stabilizes the *CO_2 state and lowers the Tafel slope.[1] Hence, a more negative zeta potential for PdZnGCN corroborates its better catalytic performance, enhanced kinetics, and, consequently, higher TOF and FE.[1]

Adsorption tests were carried out using PdZnGCN, PdZn, and GCN catalysts. The result indicates that the amount of CO_2 adsorbed followed the order with PdZnGCN (4.33 cm^3/g) > GCN (3.32 cm^3/g) > PdZn (2.20 cm^3/g), whereas the amount of CO desorbed was PdZnGCN (1.18 cm^3/g) > PdZn (1.04 cm^3/g) > GCN (0.76 cm^3/g), as summarized in Table S6. These results demonstrate that the CO desorption rate of PdZnGCN is higher than PdZn and GCN resulting in higher catalytic activity and selectivity of the product.[44]

To further elaborate on the effect of electronic tuning via compressive strain, the ECO_2RR mechanism at the surface for both PdZn and PdZnGCN is depicted in Figure 5. This diagram correlates the binding strength of COOH, CO, and H intermediates with the positions of d-band centers (ε_d) relative to the Fermi levels. For PdZn without CO_2 and with CO_2, the ε_d is close to the E_F, which corresponds to strong binding strengths of COOH and CO, indicating that activation of CO_2 by stabilizing COOH intermediates and adsorbed CO formation is adequate. Nonetheless, the desorption of CO from the surface is limited due to the strongest binding strength of CO on Pd. However, under an applied potential of −1.5 V versus Ag/AgCl in the presence of CO_2, the ε_d of the PdZnGCN composite is more downshifted than PdZn, which induces weak binding strength for CO and results in an increased electrocatalytic CO_2 to CO conversion at a faster rate.[45] Consequently, the superior performance of PdZnGCN over the individual PdZn and GCN is due to the synergistic electronic interaction between the GCN and PdZn components as seen in XPS, Fourier transformed infrared (FTIR), and XANES. This interaction and the reduced size of PdZn nanoparticles as seen in SEM and TEM when composited with GCN produce a compressive strain that increases the active surface area, downshifts the d-band center, and alters the surface WF. Moreover, this tuning further modifies the zeta potential and CO sorption properties to further reduce the activation energy for CO_2 reduction and prevent the catalyst poisoning from accumulated CO adsorption. This leads to facile desorption and improved selectivity of the CO product, as evident from higher FE, higher exchange current density, higher TOF, lower Tafel slope, and lower charge transfer resistance for PdZnGCN.

Based on the kinetics of the electrode surface using Tafel plots, the electrocatalytic mechanism on its surface pathway is as follows

$$CO_2 + e^- \leftrightarrow *CO_2^- \tag{1}$$

$$CO_{2(g)} + H^+_{(aq)} + e^- \rightarrow \text{*COOH} \tag{2}$$

$$\text{*COOH} + H^+_{(aq)} + e^- \rightarrow \text{*CO} + H_2O_{(l)} \tag{3}$$

$$\text{*CO} \rightarrow CO_{(g)} \tag{4}$$

where * denotes the adsorbed molecule on the electrode.

■ EXPERIMENTAL SECTION

Synthesis for Bulk and Nanosheet g-C_3N_4. The bulk graphitic carbon nitride was synthesized by directly heating a precursor, dicyandiamide (Acros Organics, 99.5%), by taking 2 g (23.79 mmol) in a porcelain crucible covered with a lid and heating it to 350 °C at the rate of 4 °C/min in a muffle furnace. The temperature was maintained for additional 2 h at 600 °C at the rate of 3 °C/min. After cooling down, the yellow powder product was collected and labeled as bulk g-C_3N_4. The graphitic carbon nitride nanosheet was synthesized using chemical exfoliation techniques by taking (1 g) of bulk g-C_3N_4, mixing it with 10 mL of H_2SO_4 (98 wt %, Sigma-Aldrich) in a round-bottom flask, and stirring it for 8 h at room temperature. The mixture was slowly poured into 100 mL of deionized water and sonicated for exfoliation for further 2 h. The obtained suspension was centrifuged, and the collected solid was washed thoroughly with deionized water and then dried at 60 °C in a vacuum oven overnight. The obtained powder (0.5 g) was put into a flask with 150 mL of methanol and refluxed in an oil bath heater at 65 °C for 6 h. After centrifugation and drying at 60 °C in a vacuum oven, the obtained product was labeled as graphitic carbon nitride, g-C_3N_4 (GCN).[14]

Synthesis for PdZnGCN, PdGCN, ZnGCN, and PdZn. In a typical procedure, 0.5 g of the as-synthesized g-C_3N_4 was thoroughly dispersed in 25 mL of deionized water by sonication for 2 h followed by stirring at room temperature for 30 min. 4.8 mL freshly prepared sodium borohydride, 0.1 M $NaBH_4$ (98%, Acros), with a mol ratio of $NaBH_4$ to metal of 10/1, was added dropwise. The resulting dark brown precipitate was stirred for a further 1 h. A required volume of 0.004 M Pd ($CH_3COO)_2$, (Acros, 99.9%) (40 mL) and 40 mL of Zn ($CH_3COO)_2$·2H_2O (Showa, 99%) with 0.002 M salt solution was added dropwise with continuous stirring. The mixture was transferred to a 20 mL Teflon-lined autoclave and heated at 160 °C for 12 h. Subsequently, after cooling to room temperature, the precipitate was centrifuged at 4000 rpm, washed with ethanol, and deionized water several times, and dried at 60 °C for 12 h. Finally, the obtained composite was grounded and labeled as PdZnGCN. For the synthesis of PdGCN and ZnGCN, 0.5 g of the as-synthesized GCN was thoroughly dispersed in 25 mL of deionized water by sonication for 2 h, followed by stirring at room temperature for 30 min. The solution was added dropwise under continuous stirring with 40 mL of 0.004 M Pd($CH_3COO)_2$ (Acros, 99.9%) or 40 mL of 0.002 M Zn($CH_3COO)_2$·2H_2O (Showa, 99%). 4.8 mL of freshly prepared 0.1 M $NaBH_{4(aq)}$ (98%, Acros) was added dropwise. The resulting dark brown precipitate for PdGCN (and yellowish precipitate for ZnGCN) was stirred for a further 1 h. The mixture was transferred into four 20 mL Teflon-lined autoclaves and heated at 160 °C for 12 h. After cooling to room temperature, the product was combined and centrifuged at 4000 rpm to collect the solid precipitate, washed with ethanol and deionized water several times, and dried at 60 C for 12 h. Finally, the obtained composite was grounded and labeled as PdGCN and ZnGCN,

respectively. Similarly, PdZn was prepared by adding the solution of 0.004 M Pd($CH_3COO)_2$ (Acros, 99.9%) and 0.002 M Zn($CH_3COO)_2$·2H_2O (Showa, 99%). Then, 4.8 mL of freshly prepared 0.1 M $NaBH_{4(aq)}$ (98%, Acros) was added dropwise. The resulting dark brown precipitate was stirred for a further 1 h. The mixture was transferred into five 20 ml Teflon-lined autoclaves and heated at 160 °C for 12 h. After cooling to room temperature, the product was combined and centrifuged at 4000 rpm to collect the solid precipitate, washed with ethanol and deionized water several times, and dried at 60 °C for 12 h. Finally, the obtained composite was grounded and labeled as PdZn.[44]

Structural Characterizations. XRD measurements were conducted using a Bruker D8 Advance X-ray diffractometer at 40 kV using monochromatized Cu K_α (λ = 1.5406 Å) radiation in the 2θ range of 10−80°. The morphologies of the materials were determined using a Zeiss Gemini Ultra Plus field-emission scanning electron microscope (FESEM) operated at an accelerating voltage of 0.02−30 kV and a 200 kV JEOL HRTEM. XPS was used to analyze surface properties equipped with Al K_α as a radiation source on an ULVAC PHI Quantera II high-resolution XPS. The work function and d-band measurements were performed with a full-field soft X-ray tomography beamline 24A of the Taiwan Photon Source (TPS) at the National Synchrotron Radiation Research Center (NSRRC). EXAFS was recorded with the 17C wiggler beamline of the Taiwan Light Source (TLS) or XRD beamlines 20A and 44A of TPS at NSRRC. FTIR spectra were recorded on a Bruker VERTEX 700 spectrometer with a wavelength range between 4000 and 400 cm^{-1}. Elemental analyses were obtained by -EDX, 200 kV, JEOL, USA) and ICP-OES, (PerkinElmer, SCIEX Elan 500). The zeta potential (ζ) was measured using a Malvern Zetasizer, and adsorption studies were performed using Micrometrics 3Flex.

Electrochemical Characterizations. The following procedures were applied to fabricate working electrodes. The as-synthesized GCN, PdZnGCN, and PdZn (10 mg of each) were dispersed in a mixed solution containing 0.1 mL of 5 wt % Nafion solutions, 0.2 mL of distilled water, and 0.3 mL of isopropanol, respectively. Using the drop casting method, a 150 μL aliquot of this suspension was coated onto a carbon cloth substrate (1.5 × 1 cm^2). The electrodes were then dried at 60 °C under vacuum. The average masses from three samples were 2.11 ± 0.13, 2.08 ± 0.17, and 2.09 ± 0.11 mg for GCN, PdZnGCN, and PdZn electrodes, respectively. Cyclic voltammetry measurements, LSV, EIS, and bulk electrolysis experiments were conducted in 40 mL of 0.1 M KCl aqueous electrolytic solutions. KCl was used as a working electrolyte rather than KHCO$_3$ because the solubility of CO$_2$ in the low concentration of KCl increases due to the salting-out effect, which generates a high CO$_2$ reduction current. EIS was measured using a ZIVE LAB electrochemical working station, and the fitting was carried out with the software ZIVE SM Version 6.687 using the equivalent circuit model described in Figure S14. The frequency range for measurement was 1 MHz to 1 kHz. Electrochemical CO$_2$ reduction reactions (ECO$_2$RR) were carried out with an electrochemical workstation (CHI-660E) using a three-electrode system with a catalyst coated on carbon cloth as the working electrode and Ag/AgCl (in 3.0 M KCl) and a platinum coiled wire as the reference and counter electrodes, respectively, with a scan rate of 0.1 V/s. The Tafel plots were derived from LSV with a scan rate of 0.05 V/s. A custom-made two-compartment H-cell partition with a proton

exchange membrane was used to separate the working electrode and the counter electrode ([Figure S17](#)). The headspace gaseous products of electrochemical CO_2 reduction reactions were analyzed by GC (Agilent 7890B) equipped with a TCD through manual injection.

CONCLUSIONS

In summary, we prepared a novel PdZnGCN nanocomposite via a simple hydrothermal route and employed it for ECO$_2$RR. The as-fabricated PdZnGCN electrode exhibited superior selectivity of 95.4% for CO at an applied potential of −0.9 V versus RHE (−1.5 V vs Ag/AgCl) with a high CO partial current density of 4.4 mA cm^{-2} and Faradaic efficiencies of 93.6% for CO and 4.5% for H$_2$. The TOF value for PdZnGCN reached an average value of 20 974 h^{-1} which is much higher than PdZn (2772 h^{-1}) and GCN (1261 h^{-1}) at 1 h and was considerably higher than most of the current state-of-the-art catalysts. The steady current density and linearly increased charge accumulation after long-term electrolysis as well as consecutive electrolysis demonstrated that PdZnGCN exhibited good stability and recyclable stability. The enhanced activity of PdZnGCN electrodes with high partial current density and FE simultaneously was attributed to the enhanced charge transfer process at the interface and the higher electrochemically active surface area, indicating more active sites due to the synergistic effect. Moreover, the strain-induced downward shift of the d-band center and the optimum work function value facilitated the enhanced selectivity for CO. This work provides an example of utilizing strain and synergistic effects to tune the catalytic properties for electrochemical reduction of CO$_2$. Hence, a rational design of an efficient and affordable bimetallic g-C$_3$N$_4$ nanocomposite with desired characteristics can be potentially achieved for the mass production of CO as a feedstock of energy-dense fuels and chemicals.

ASSOCIATED CONTENT

Supporting Information

The Supporting Information is available free of charge at https://pubs.acs.org/doi/10.1021/acsomega.2c01216.

> Additional experimental details, photographs of the experimental setup, SEM, TEM mapping, quantification results, Nyquist plots, and related tables interpreting quantification and fitting results ([PDF](#))

AUTHOR INFORMATION

Corresponding Authors

Mohammad Rameez − *Institute of Chemistry, Academia Sinica, Taipei 115201, Taiwan;* orcid.org/0000-0003-4712-9584; Email: mdakhnatan@gmail.com

Chen-Hsiung Hung − *Institute of Chemistry, Academia Sinica, Taipei 115201, Taiwan;* orcid.org/0000-0002-8060-348X; Email: chhung@gate.sinica.edu.tw

Authors

Girma W. Woyessa − *Sustainable Chemical Science and Technology, Taiwan International Graduate Program, Taipei 115201, Taiwan; Department of Applied Chemistry, National Yang Ming Chiao Tung University, Hsinchu 300093, Taiwan; Institute of Chemistry, Academia Sinica, Taipei 115201, Taiwan*

Chuan-Hung Chuang − *Institute of Chemistry, Academia Sinica, Taipei 115201, Taiwan*

Complete contact information is available at:
https://pubs.acs.org/10.1021/acsomega.2c01216

Notes

The authors declare no competing financial interest.

ACKNOWLEDGMENTS

REFERENCES

(1) Tan, X.; Yu, C.; Song, X.; Zhao, C.; Cui, S.; Xu, H.; Chang, J.; Guo, W.; Wang, Z.; Xie, Y.; Qiu, J. Toward an Understanding of the Enhanced CO$_2$ Electroreduction in NaCl Electrolyte over CoPc Molecule-Implanted Graphitic Carbon Nitride Catalyst. *Adv. Energy Mater.* **2021**, *11*, 2100075.

(2) Xue, D.; Xia, H.; Yan, W.; Zhang, J.; Mu, S. Defect Engineering on Carbon-Based Catalysts for Electrocatalytic CO$_2$ Reduction. *Nano-Micro Lett.* **2021**, *13*, 5.

(3) Rosen, J.; Hutchings, G. S.; Lu, Q.; Forest, R. V.; Moore, A.; Jiao, F. Electrodeposited Zn Dendrites with Enhanced CO Selectivity for Electrocatalytic CO$_2$ Reduction. *ACS Catal.* **2015**, *5*, 4586−4591.

(4) Albo, J.; Alvarez-Guerra, M.; Castaño, P.; Irabien, A. Towards the Electrochemical Conversion of Carbon Dioxide into Methanol. *Green Chem.* **2015**, *17*, 2304−2324.

(5) Li, C.; Shen, G.; Zhang, R.; Wu, D.; Zou, C.; Ling, T.; Liu, H.; Dong, C.; Du, X.-W. Zn Nanosheets Coated with a ZnS Sub nanometer Layer for Effective and Durable CO$_2$ Reduction. *J. Mater. Chem. A* **2019**, *7*, 1418−1423.

(6) Liu, K.; Wang, J.; Shi, M.; Yan, J.; Jiang, Q. Simultaneous Achieving of High Faradaic Efficiency and CO Partial Current Density for CO$_2$ Reduction via Robust, Noble-Metal-Free Zn Nanosheets with Favorable Adsorption Energy. *Adv. Energy Mater.* **2019**, *9*, 1900276.

(7) Zheng, Y.; Jiao, Y.; Zhu, Y.; Li, L. H.; Han, Y.; Chen, Y.; Du, A.; Jaroniec, M.; Qiao, S. Z. Hydrogen Evolution by a Metal-Free Electrocatalyst. *Nat. Commun.* **2014**, *5*, 3783.

(8) Zheng, Y.; Jiao, Y.; Chen, J.; Liu, J.; Liang, J.; Du, A.; Zhang, W.; Zhu, Z.; Smith, S. C.; Jaroniec, M.; Lu, G. Q.; Qiao, S. Z. Nanoporous Graphitic-C$_3$N$_4$ @Carbon Metal-Free Electrocatalysts for Highly Efficient Oxygen Reduction. *J. Am. Chem. Soc.* **2011**, *133*, 20116−20119.

(9) Zhang, B.; Zhao, T.-J.; Feng, W.-J.; Liu, Y.-X.; Wang, H.-H.; Su, H.; Lv, L.-B.; Li, X.-H.; Chen, J.-S. Polarized Few-Layer g-C$_3$N$_4$ as Metal-Free Electrocatalyst for Highly Efficient Reduction of CO$_2$. *Nano Res.* **2018**, *11*, 2450−2459.

(10) Samanta, S.; Srivastava, R. Catalytic Conversion of CO$_2$ to Chemicals and Fuels: The Collective Thermo-catalytic/Photo-catalytic/Electrocatalytic Approach with Graphitic Carbon Nitride. *Mater. Adv.* **2020**, *1*, 1506−1545.

(11) Jiao, Y.; Zheng, Y.; Chen, P.; Jaroniec, M.; Qiao, S.-Z. Molecular Scaffolding Strategy with Synergistic Active Centers to Facilitate Electrocatalytic CO$_2$ Reduction to Hydrocarbon/Alcohol. *J. Am. Chem. Soc.* **2017**, *139*, 18093−18100.

(12) Lu, X.; Tan, T. H.; Ng, Y. H.; Amal, R. Highly Selective and Stable Reduction of CO$_2$ to CO by a Graphitic Carbon Nitride/Carbon Nanotube Composite Electrocatalyst. *Chem.—Eur. J.* **2016**, *22*, 11991−11996.

(13) Chen, J.; Wang, Z.; Lee, H.; Mao, J.; Grimes, C. A.; Liu, C.; Zhang, M.; Lu, Z.; Chen, Y.; Feng, S.-P. Efficient Electroreduction of CO_2 to CO by Ag-Decorated S-Doped g-C_3N_4/CNT Nanocomposites at Industrial Scale Current Density. *Mater. Today Phys.* **2020**, *12*, 100176.

(14) Woyessa, G. W.; dela Cruz, J.-a. B.; Rameez, M.; Hung, C.-H. Nanocomposite Catalyst of Graphitic Carbon Nitride and Cu/Fe Mixed Metal Oxide for Electrochemical CO_2 Reduction to CO. *Appl. Catal., B* **2021**, *291*, 120052.

(15) Valenti, M.; Prasad, N. P.; Kas, R.; Bohra, D.; Ma, M.; Balasubramanian, V.; Chu, L.; Gimenez, S.; Bisquert, J.; Dam, B.; Smith, W. A. Suppressing H_2 Evolution and Promoting Selective CO_2 Electroreduction to CO at Low Overpotentials by Alloying Au with Pd. *ACS Catal.* **2019**, *9*, 3527−3536.

(16) Zeng, J.; Zhang, W.; Yang, Y.; Li, D.; Yu, X.; Gao, Q. Pd−Ag Alloy Electrocatalysts for CO_2 Reduction: Composition Tuning to Break the Scaling Relationship. *ACS Appl. Mater. Interfaces* **2019**, *11*, 33074−33081.

(17) Kitchin, J. R.; Nørskov, J. K.; Barteau, M. A.; Chen, J. G. Role of Strain and Ligand Effects in the Modification of the Electronic and Chemical Properties of Bimetallic Surfaces. *Phys. Rev. Lett.* **2004**, *93*, 156801.

(18) Xia, Z.; Guo, S. Strain Engineering of Metal-Based Nanomaterials for Energy Electrocatalysis. *Chem. Soc. Rev.* **2019**, *48*, 3265−3278.

(19) Gunji, T.; Ochiai, H.; Ohira, T.; Liu, Y.; Nakajima, Y.; Matsumoto, F. Preparation of Various Pd-Based Alloys for Electrocatalytic CO_2 reduction Reaction - Selectivity Depending on Secondary Elements. *Chem. Mater.* **2020**, *32*, 6855−6863.

(20) Yin, Z.; Gao, D.; Yao, S.; Zhao, B.; Cai, F.; Lin, L.; Tang, P.; Zhai, P.; Wang, G.; Ma, D.; Bao, X. Highly Selective Palladium-Copper Bimetallic Electrocatalysts for the Electrochemical Reduction of CO_2 to CO. *Nano Energy* **2016**, *27*, 35−43.

(21) Chen, X.; Hou, Y.; Wang, H.; Cao, Y.; He, J. Facile Deposition of Pd Nanoparticles on Carbon Nanotube Microparticles and Their Catalytic Activity for Suzuki Coupling Reactions. *J. Phys. Chem. C* **2008**, *112*, 8172−8176.

(22) Gracia-Espino, E.; Hu, G.; Shchukarev, A.; Wågberg, T. Understanding the Interface of Six-Shell Cuboctahedral and Icosahedral Palladium Clusters on Reduced Graphene Oxide: Experimental and Theoretical Study. *J. Am. Chem. Soc.* **2014**, *136*, 6626−6633.

(23) Mai, N. T.; Thuy, T. T.; Mott, D. M.; Maenosono, S. Chemical Synthesis of Blue-Emitting Metallic Zinc Nano-Hexagons. *CrystEngComm* **2013**, *15*, 6606.

(24) Pankhurst, J. R.; Guntern, Y. T.; Mensi, M.; Buonsanti, R. Molecular Tunability of Surface-Functionalized Metal Nanocrystals for Selective Electrochemical CO_2 Reduction. *Chem. Sci.* **2019**, *10*, 10356−10365.

(25) Wang, W.; Zhang, H.; Zhang, S.; Liu, Y.; Wang, G.; Sun, C.; Zhao, H. Potassium-Ion-Assisted Regeneration of Active Cyano Groups in Carbon Nitride Nanoribbons: Visible-Light-Driven Photocatalytic Nitrogen Reduction. *Angew. Chem., Int. Ed.* **2019**, *58*, 16644−16650.

(26) Ray, S. C.; Pao, C. W.; Chiou, J. W.; Tsai, H. M.; Jan, J. C.; Pong, W. F.; McCann, R.; Roy, S. S.; Papakonstantinou, P.; McLaughlin, J. A. Electronic properties of a-CNx thin films: An x-ray-absorption and photoemission spectroscopy study. *J. Appl. Phys.* **2005**, *98*, 033708.

(27) Zhang, C.; Yang, S.; Wu, J.; Liu, M.; Yazdi, S.; Ren, M.; Sha, J.; Zhong, J.; Nie, K.; Jalilov, A. S.; Li, Z.; Li, H.; Yakobson, B. I.; Wu, Q.; Ringe, E.; Xu, H.; Ajayan, P. M.; Tour, J. M. Electrochemical CO_2 Reduction with Atomic Iron-Dispersed on Nitrogen-Doped Graphene. *Adv. Energy Mater.* **2018**, *8*, 1703487.

(28) Lee, J. H.; Ryu, J.; Kim, J. Y.; Nam, S.-W.; Han, J. H.; Lim, T.-H.; Gautam, S.; Chae, K. H.; Yoon, C. W. Carbon Dioxide Mediated, Reversible Chemical Hydrogen Storage Using a Pd Nanocatalyst Supported on Mesoporous Graphitic Carbon Nitride. *J. Mater. Chem. A* **2014**, *2*, 9490.

(29) Deng, F.; Huang, J.; Ember, E. E.; Achterhold, K.; Dierolf, M.; Jentys, A.; Liu, Y.; Pfeiffer, F.; Lercher, J. A. On the Mechanism of Catalytic Decarboxylation of Carboxylic Acids on Carbon-Supported Palladium Hydride. *ACS Catal.* **2021**, *11*, 14625−14634.

(30) Erat, S.; Ozkendir, O. M.; Yildirimcan, S.; Gunaydin, S.; Harfouche, M.; Demir, B.; Braun, A. Study on Crystallographic and Electronic Structure of Micrometre-Scale ZnO and ZnO:B Rods via X-Ray Absorption Fine-Structure Spectroscopy. *J. Synchrotron Radiat.* **2021**, *28*, 448−454.

(31) Shah, A. H.; Wang, Y.; Hussain, S.; Akbar, M. B.; Woldu, A. R.; Zhang, X.; He, T. New Aspects of C2 Selectivity in Electrochemical CO_2 Reduction over Oxide-Derived Copper. *Phys. Chem. Chem. Phys.* **2020**, *22*, 2046−2053.

(32) Liu, G.; Niu, P.; Sun, C.; Smith, S. C.; Chen, Z.; Lu, G. Q.; Cheng, H.-M. Unique Electronic Structure Induced High Photoreactivity of Sulfur-Doped Graphitic C_3N_4. *J. Am. Chem. Soc.* **2010**, *132*, 11642−11648.

(33) Li, C.; Yan, S.; Fang, J. Construction of Lattice Strain in Bimetallic Nanostructures and Its Effectiveness in Electrochemical Applications. *Small* **2021**, *17*, 2102244.

(34) Bao, M.; Chen, X.; Hu, S.; Zhang, L.; Li, Y.; Carraro, C.; Maboudian, R.; Wei, W.; Zhang, Y.; Liu, S. Atomically Ordered Intermetallic PdZn Coupled with Co Nanoparticles as a Highly Dispersed Dual Catalyst Chemically Bonded to N-Doped Carbon for Boosting Oxygen Reduction Reaction Performance. *J. Mater. Chem. A* **2020**, *8*, 21327−21338.

(35) Zhu, Y.; Lv, K.; Wang, X.; Yang, H.; Xiao, G.; Zhu, Y. 1D/2D Nitrogen-Doped Carbon Nanorod Arrays/Ultrathin Carbon Nanosheets: Outstanding Catalysts for the Highly Efficient Electroreduction of CO_2 to CO. *J. Mater. Chem. A* **2019**, *7*, 14895−14903.

(36) Lv, W.; Zhang, R.; Gao, P.; Lei, L. Studies on the Faradaic Efficiency for Electrochemical Reduction of Carbon Dioxide to Formate on Tin Electrode. *J. Power Sources* **2014**, *253*, 276−281.

(37) Lamaison, S.; Wakerley, D.; Blanchard, J.; Montero, D.; Rousse, G.; Mercier, D.; Marcus, P.; Taverna, D.; Giaume, D.; Mougel, V.; Fontecave, M. High-Current-Density CO_2-to-CO Electroreduction on Ag-Alloyed Zn Dendrites at Elevated Pressure. *Joule* **2020**, *4*, 395−406.

(38) Abbasi, P.; Asadi, M.; Liu, C.; Sharifi-Asl, S.; Sayahpour, B.; Behranginia, A.; Zapol, P.; Shahbazian-Yassar, R.; Curtiss, L. A.; Salehi-Khojin, A. Tailoring the Edge Structure of Molybdenum Disulfide toward Electrocatalytic Reduction of Carbon Dioxide. *ACS Nano* **2017**, *11*, 453−460.

(39) Gao, D.; Zhou, H.; Wang, J.; Miao, S.; Yang, F.; Wang, G.; Wang, J.; Bao, X. Size-Dependent Electrocatalytic Reduction of CO_2 over Pd Nanoparticles. *J. Am. Chem. Soc.* **2015**, *137*, 4288−4291.

(40) Han, Z.; Choi, C.; Tao, H.; Fan, Q.; Gao, Y.; Liu, S.; Robertson, A. W.; Hong, S.; Jung, Y.; Sun, Z. Tuning the Pd-Catalyzed Electroreduction of CO_2 to CO with Reduced Overpotential. *Catal. Sci. Technol.* **2018**, *8*, 3894−3900.

(41) Zeng, M.; Li, Y. Recent Advances in Heterogeneous Electrocatalysts for the Hydrogen Evolution Reaction. *J. Mater. Chem. A* **2015**, *3*, 14942−14962.

(42) Su, T.; Li, Y.; Xue, S.; Xu, Z.; Zheng, M.; Xia, C. Kinetics of CO_2 Electrolysis on Composite Electrodes Consisting of Cu and Samaria-Doped Ceria. *J. Mater. Chem. A* **2019**, *7*, 1598−1606.

(43) Medina-Ramos, J.; DiMeglio, J. L.; Rosenthal, J. Efficient Reduction of CO_2 to CO with High Current Density Using *in situ* or *ex situ* Prepared Bi-Based Materials. *J. Am. Chem. Soc.* **2014**, *136*, 8361−8367.

(44) Majeed, I.; Manzoor, U.; Kanodarwala, F. K.; Nadeem, M. A.; Hussain, E.; Ali, H.; Badshah, A.; Stride, J. A.; Nadeem, M. A. Pd−Ag Decorated g-C_3N_4 as an Efficient Photocatalyst for Hydrogen Production from Water under Direct Solar Light Irradiation. *Catal. Sci. Technol.* **2018**, *8*, 1183−1193.

(45) Ma, M.; Hansen, H. A.; Valenti, M.; Wang, Z.; Cao, A.; Dong, M.; Smith, W. A. Electrochemical Reduction of CO_2 on Compositionally Variant Au-Pt Bimetallic Thin Films. *Nano Energy* **2017**, *42*, 51−57.